Absence of half-metallicity in defect-free digital magnetic heterostructures δ-doped with Cr and Mn

F. Beiuşeanu,[1] C. Horea,[1] E.-V. Macocian,[1] T. Jurcuţ,[1] L. Vitos,[2,3,4] and L. Chioncel[5,6]

[1]*Department of Physics, University of Oradea, RO-410087 Oradea, Romania*

[2]*Applied Materials Physics, Department of Materials Science and Engineering, Royal Institute of Technology, Stockholm SE-100 44, Sweden*

[3]*Department of Physics and Materials Science, Uppsala University, PO Box 516, SE-75120 Uppsala, Sweden*

[4]*Research Institute for Solid State Physics and Optics, Budapest H-1525, PO Box 49, Hungary*

[5]*Augsburg Center for Innovative Technologies, University of Augsburg, D-86135 Augsburg, Germany*

[6]*Theoretical Physics III, Center for Electronic Correlations and Magnetism, Institute of Physics, University of Augsburg, D-86135 Augsburg, Germany*

(Received 1 October 2010; revised manuscript received 3 February 2011; published 18 March 2011)

We present the results of combined density functional and many-body calculations of the electronic and magnetic properties of the defect-free digital ferromagnetic heterostructures obtained by doping GaAs with Cr and Mn. While the local-density approximation $+U$ predicts half-metallicity in these defect-free delta-doped heterostructures, we demonstrate that local many-body correlations captured by dynamical mean-field theory induce within the minority-spin channel nonquasiparticle states just above E_F. As a consequence of the existence of these many-body states the half-metallic gap is closed and the carriers' spin polarization is significantly reduced. Below the Fermi level the minority-spin highest valence states are found to localize more on the GaAs layers, being independent of the type of electronic correlations considered. Thus, our results confirm the confinement of carriers in these delta-doped heterostructures, having a spin polarization that follows a different temperature dependence than the magnetization. We suggest that polarized hot-electron photoluminescence experiments might uncover evidence for the existence of many-body states within the minority-spin channel and elucidate their finite-temperature behavior.

DOI: 10.1103/PhysRevB.83.125107 PACS number(s): 75.50.Cc, 71.10.Fd, 71.20.−b, 71.27.+a

I. INTRODUCTION

Digital magnetic heterostructures (DMHs) are semiconductor heterostructures in which magnetic monolayers are incorporated using the digital-alloy technique.[1,2] This technique was developed in order to combine conventional semiconductors with magnetic materials, with the desire to realize simultaneous band-gap and magnetic engineering. Within the DMH technique, the quality of magnetic monolayers is highly sensitive to growth conditions, similarly to the case of diluted magnetic semiconductors, where low-temperature thermal annealing[3,4] and codoping[5,6] have been extensively developed. Therefore, the existing technological difficulties increase the significance of a first-principles investigation, which can predict many characteristics of DMHs and indicate trends in their properties.

For DMH materials, most first-principles investigations were done for Mn-doped GaAs.[7,8] The exchange interactions inside and between Mn monolayers were analyzed; in particular, the spacer-dependent magnetic properties were recently discussed.[9] Independent of the spacer thickness, the electronic structure was predicted to be half-metallic and, using the technique of injection of free holes,[10] intra- and interlayer exchange coupling mechanisms were discussed.[9] In addition, previous studies discussed transport properties, optimal concentration of Mn, possible effects of antisite defects, etc.[7,8] A number of calculations were also performed for Mn-doped Si, Ge, and Ga.[11–13]

Properties of these heterostructures are expected to deviate from the physical behavior presented by the family of diluted magnetic semiconductors.[14] The most common position occupied by Mn within the (III,V) host GaAs diluted magnetic semiconductor is the Ga site. The substitutional Mn contributes with its two 4*s* electrons in the crystal bonding similarly as the two Ga 4*s* electrons. Less favorable energetically is the interstitial Mn position, so it is less common.[14] While in Mn-doped GaAs semiconductors the system is described as "bulk," in the fabrication of Mn-doped GaAs digital magnetic heterostructures, MnAs monolayers were embedded into GaAs superlattices,[15] so that the quasibidimensional geometry of the MnAs layer is preserved. Thus, the random substitution of positions (Ga-occupied or interstitial) by the Mn ions in the case of diluted magnetic semiconductors shows up as an ordered replacement of GaAs layers by MnAs layers in the case of DMH, with evident consequences upon the critical temperature. DMH exhibits an unexpected Curie-temperature dependence on the concentration of Mn ions. At a fixed Mn concentration (fixed number of MnAs layers), the Curie temperature decreases with the thickness of the GaAs, but saturates at large thicknesses ($\cong$50 GaAs monolayers).[15] Electronic structure calculations were also reported in the literature for the case of δ doping with Mn of GaAs/AlAs superlattices.[7] In the defect-free cases, a half-metallic heterostructure was obtained. It was also demonstrated that, in the presence of As antisites, the half-metallic state was destroyed and a *p*-type metallic conductance was evidenced because of the majority-spin electrons. In addition, the computed magnetic coupling between the Mn ions becomes larger in the presence of As antisites.[7] To the best of our knowledge, no results which include electronic correlations were reported for the case of Cr or Mn, even in the defect-free case.

In this paper we present results of the first-principles electronic structure calculations within the local spin density

approximation (LSDA), LSDA + U, and LSDA + dynamical mean-field theory (DMFT) for the different defect-free $(M\mathrm{As})_1/(\mathrm{GaAs})_7$ digital heterostructures containing transition-metal–arsenide monolayers (M = Cr, Mn) introduced into the GaAs superstructure. The most important correlation effect in half-metals, (i.e., the formation of many-body states within the gap) cannot be captured by the mean-field LSDA and LSDA + U type calculations. Dynamical mean-field theory was demonstrated to be able to describe such effects;[16] therefore, it is essential to directly compare the mean-field LSDA and LSDA + U and the DMFT results. We demonstrate that the half-metallic character is lost in δ-doped GaAs heterostructures containing Cr or Mn at finite temperatures and in the presence of dynamic correlations. Correlation effects soften the magnetic properties of the ferromagnetic layers, induce states above E_F with tails that cross the Fermi level, and reduce the carrier spin polarization. Within the minority-spin channel below the Fermi level the character of states forming the band edge remains unaffected by electronic correlations and the states are mostly localized on GaAs layers, confirming the experimentally observed confinement of carriers in these heterostructures.[15,17]

II. CRYSTAL STRUCTURE AND COMPUTATIONAL METHOD

To compute the electronic structure for the digital magnetic heterostructures we used the standard representation of the tetragonal symmetry: space group P-4m2. The tetragonal supercell was obtained from the fcc unit cell by a rotation in the basal plane and an integer translation along the (001) direction. The new translation vectors are $a = a_0/\sqrt{2}$, $b = a_0/\sqrt{2}$, and $c = a_0 N$, where a_0 is the bulk GaAs lattice parameter and $N = 4$, and they correspond to a $(\mathrm{GaAs})_8$ supercell. Within this supercell a GaAs monolayer is replaced by MAs, such that the obtained DMH has the unit cell formula $(M\mathrm{As})_1/(\mathrm{GaAs})_{2N-1}$. For GaAs, which has an open structure, a close-packed structure is obtained by including empty spheres. Such empty potential wells were used also in the present heterostructure geometry. We used identical muffin-tin spheres for all atoms in the unit cell having the average Wigner-Seitz radius 2.628 52 a.u., corresponding to the experimental GaAs lattice parameter ($a_0 = 5.65$ Å). The basis used for the self-consistent calculations contains the *spd* partial waves for transition metals, $sp(d)$ partial waves for Ga and As, and $s(p)$ partial waves for the empty spheres E. The notation (l) means that the l partial waves are downfolded within the self-consistent calculations. Self-consistency was performed for 105 irreducible k points and total-energy convergence was achieved with an accuracy of 10^{-6} Ry. Results for the density of states, magnetic moments, and spin polarizations are presented in the next section.

Correlation effects in the valence 3d orbitals are included via an onsite electron-electron interaction in the form $\frac{1}{2}\sum_{i\{m,\sigma\}} U_{mm'm''m'''} c^{\dagger}_{im\sigma} c^{\dagger}_{im'\sigma'} c_{im'''\sigma'} c_{im''\sigma}$. The interaction is treated in the framework of DMFT,[18–20] with a spin-polarized T-matrix fluctuation exchange (SPTF) type of impurity solver[21] implemented within the exact muffin-tin–orbitals (EMTO) basis set.[22,23] The Coulomb matrix elements $U_{mm'm''m'''}$ are expressed in the usual way[24] in terms of three Kanamori parameters U, $U' = U - 2J$, and J. Here, $c_{im\sigma}$ ($c^{\dagger}_{im\sigma}$) destroys (creates) an electron with spin σ on orbital m on lattice site i. The SPTF approximation is a multiband spin-polarized generalization of the fluctuation exchange approximation (FLEX),[25,26] but with a different treatment of particle-hole (PH) and particle-particle (PP) channels. The PP channel is described by a T-matrix approach,[27,28] giving a renormalization of the effective interaction. This effective interaction is used explicitly in the PH channel. Justifications, further developments and details of this scheme can be found in Ref. 21.

For the case of half-metallic ferromagnets (HMF), it was demonstrated[16] by model as well as by realistic electronic structure calculations that many-body effects are crucial for half-metals: they produce states with tails that cross the Fermi level so that the gap is closed and half-metallicity is lost.[29–33] The origin of these many-body nonquasiparticle (NQP) states is connected with "spin-polaron" processes: the spin-down low-energy electron excitations, which are forbidden for the HMF in the one-particle picture, turn out to be possible as superpositions of spin-up electron excitations and virtual magnons.[16,34] Spin-polaron processes are described within the SPTF approach by the fluctuation potential matrix $W^{\sigma\sigma'}(i\omega)$ with $\sigma = \pm$, defined in a similar way as in the spin-polarized FLEX approximation:[26]

$$\hat{W}(i\omega) = \begin{pmatrix} W^{++}(i\omega) & W^{+-}(i\omega) \\ W^{-+}(i\omega) & W^{--}(i\omega) \end{pmatrix}. \tag{1}$$

The essential feature here is that potential (1) is a complex energy-dependent matrix in spin space with off-diagonal elements

$$W^{\sigma,-\sigma}(i\omega) = U^m \left[\chi^{\sigma,-\sigma}(i\omega) - \chi_0^{\sigma,-\sigma}(i\omega)\right] U^m, \tag{2}$$

where U^m represents the bare vertex matrix corresponding to the transverse magnetic channel, $\chi^{\sigma,-\sigma}(i\omega)$ is an effective transverse susceptibility matrix, and $\chi_0^{\sigma,-\sigma}(i\omega)$ is the bare transverse susceptibility.[26] $i\omega$ are fermionic Matsubara frequencies and (m) corresponds to the magnetic interaction channel.[25,26] The local Green functions as well as the electronic self-energies are spin diagonal for collinear magnetic configurations. In this approximation the electronic self-energy is calculated in terms of the effective interactions in various channels. The particle-particle contribution to the self-energy was combined with the Hartree-Fock and the second-order contributions.[26] To ensure a physically transparent description, the combined particle-particle self-energy is presented by its Hartree $\Sigma^{(TH)}(i\omega)$ and Fock $\Sigma^{(TF)}(i\omega)$ types of contributions: $\Sigma(i\omega) = \Sigma^{(TH)}(i\omega) + \Sigma^{(TF)}(i\omega) + \Sigma^{(ph)}(i\omega)$ where the particle-hole contribution $\Sigma^{(ph)}$ reads

$$\Sigma^{(ph)}_{12\sigma}(i\omega) = \sum_{34\sigma'} W^{\sigma\sigma'}_{1342}(i\omega) G^{\sigma'}_{34}(i\omega). \tag{3}$$

Since the static contribution from correlations is already included in the LSDA, so-called "double-counted" terms must be subtracted. In other words, those parts of the DFT expression for the total energy that correspond to the interaction included in the Hubbard Hamiltonian have to be subtracted. Several double-counting schemes has been proposed and used for specific materials applications.[35,36] It has been recognized that the results of the LSDA + U calculations may depend

crucially on the choice of the scheme used.[37] In particular for the class of moderately correlated metals, as one may consider the HMF in the LSDA + U calculations performed here, we used the "around-mean-field"[37] double-counting scheme. Similarly to the LSDA + U in the DMFT approach, the Hubbard Hamiltonian represents the underlying physics, while, in contrast to the mean-field LSDA + U solution, the time-dependent dynamics are considered while spatial fluctuations are neglected. Obviously, the double-counting correction has to be considered also. To achieve this, we replace $\Sigma_\sigma(E)$ with $\Sigma_\sigma(E) - \Sigma_\sigma(0)$[38] in all equations of the DMFT procedure.[19] Physically, this is related to the fact that DMFT only adds dynamical correlations to the LSDA result. For this reason, it is believed that this kind of double-counting subtraction "$\Sigma(0)$" is more appropriate for a DMFT treatment of metals than the alternative static "Hartree-Fock" (HF) subtraction.[37]

III. RESULTS AND DISCUSSION

When the monolayer of MAs, with M = Cr, Mn is introduced in the GaAs supercell, the symmetry lowering from cubic to tetragonal takes place and the 3d-t_{2g} states split further into a double-degenerate d_{xz} and d_{yz}, situated at lower energies, and the nondegenerate d_{xy}. At higher energies are situated d_{3z^2-1} and $d_{x^2-y^2}$.[24,39] Magnetic exchange interactions split the spin channels and contribute additionally to the crystal field in opening the minority-spin gap. In Fig. 1 we present spin resolved, total density of states (DOS), for the DMH structures $(M\text{As})_1/(\text{GaAs})_7$, M = Cr, Mn. In both minority- and majority-spin channels at an energy of about −12 eV (not shown in Fig. 1) the As 4s and Ga 4s are present. In the energy range −8 to −2 eV As p and Ga p states are dominant characters in the p-d bonding orbitals, while in the vicinity of the Fermi level in the energy range of −2 to 2 eV the dominant 3d transition-metal states are present (see also orbital projected DOS of Fig. 2). At the LSDA level, the occupied minority-spin channel for both compounds is similar because, in this energy range, the transition-metal d states are weakly present within the p-d bonding orbital dominated by As and Ga p states. The Fermi level is situated, for minority-spin electrons, within the gap, closer to the bottom of the conduction band. The energy gaps are $\Delta_{\text{Cr}}^{\text{LSDA}} \cong 0.51$ eV and $\Delta_{\text{Mn}}^{\text{LSDA}} \cong 0.42$ eV. The difference between the Fermi level and the bottom of the conduction band is somewhat larger for the DMH with Cr, in comparison with the value obtained in the Mn-based DMH. Given the fact that the top of the minority-spin valence band is situated at similar energies in these heterostructures, the magnitude of the gap is therefore determined by the energy distance between the Fermi level and the bottom of the conduction band.

A more detailed analysis of the density of states can be made on the basis of the orbital projected densities of states (see Fig. 2). Here the LSDA and the LSDA + U results for the correlated transition-metal atoms are compared. LSDA + U calculations were performed for different values of the average Coulomb interaction U = 2, 3, 4, and 5 eV, taking the same value for the exchange parameter of J = 0.9 eV. In Fig. 2 we show the results for U = 3 eV and J = 0.9 eV, which are typical values for transition metals.[24,40] The left column

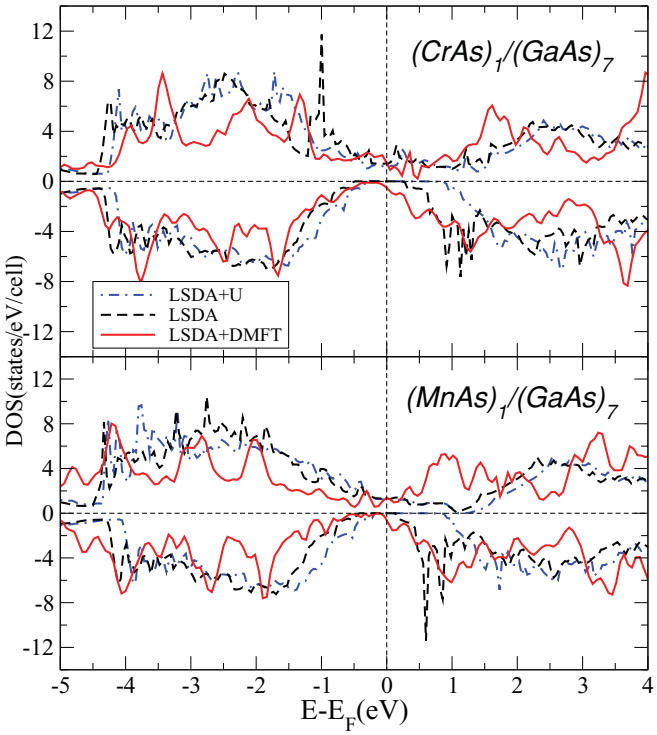

FIG. 1. (Color online) Spin-resolved total DOS of $(M\text{As})_1/(\text{GaAs})_7$, with M = Cr and Mn. The half-metallic character is evidenced by the simultaneous presence of a metallic majority-spin and an insulating (semiconducting) minority-spin DOS obtained within LSDA (dashed black line) and LSDA + U (dot-dashed blue line) calculations. Dynamical correlations captured by DMFT (solid red line) introduce many-body states within the gap that destroy half-metallicity.

represents the results for the compound with Cr, while the right column shows the densities for the compound containing Mn. In each panel the upper (lower) part contains the results for the majority (minority) spins. Although the similarities of the orbital projected DOS are visible, we note the general tendency of the LSDA + U; namely, to enlarge the minority-spin gap $\Delta_{\text{Cr}}^{\text{LSDA}+U} \cong 0.85$ eV and $\Delta_{\text{Mn}}^{\text{LSDA}+U} \cong 0.81$ eV. An interesting feature is that most of the spectral weight at the Fermi level is provided by the $3d_{x^2-y^2}$ orbital for both cases of Cr and Mn; however, the larger value is obtained with the Cr substitution. An almost negligible spectral weight is obtained for $3d_{xy}$ orbitals. As expected from this approach, transition-metal d states are pushed further apart from the Fermi level. In particular, for the Cr heterostructure within the majority-spin channel, the LSDA peaks (see Figs. 1 and 2) at about −1 eV are shifted to lower energies at −1.5 eV. The occupied majority-spin Mn states are within the bonding band at −3 eV are also shifted to lower energies at −4 eV. Within the minority-spin channel and for all compounds, the group of states situated around 1 eV above E_F are shifted accordingly to higher energies (see Figs. 1 and 2). For the other values of U and J a similar tendency for the DOS was obtained for both heterostructures. In the following, we plot the total As and Ga spin-resolved density of states for $(M\text{As})_1/(\text{GaAs})_7$, M = Cr, Mn. Figure 3 presents the results for Cr δ doping. The left (right) columns show the

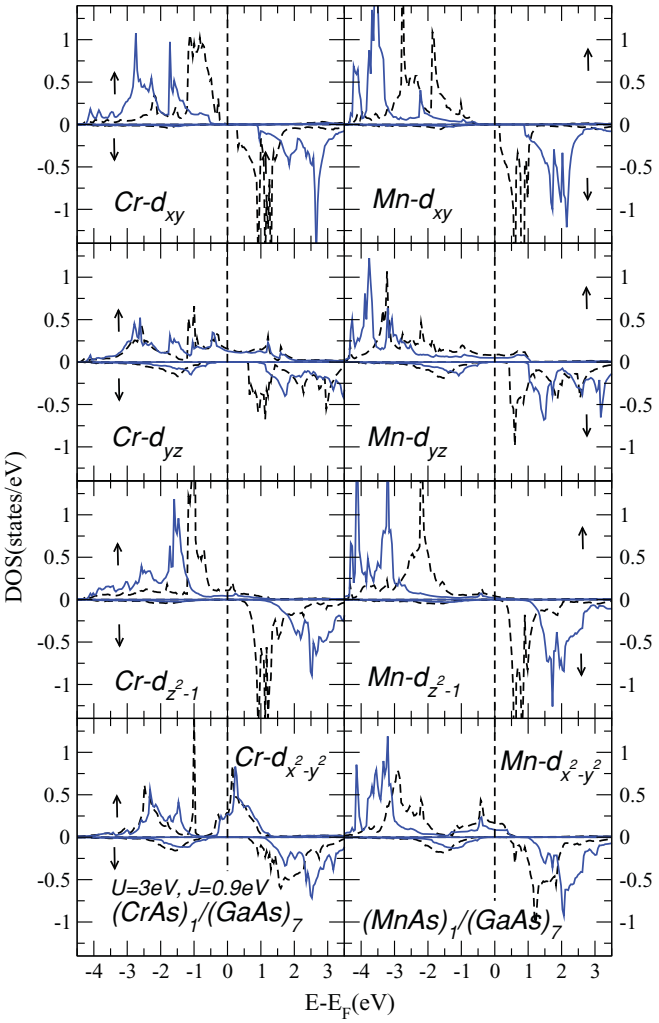

FIG. 2. (Color online) Orbital projected spin polarized DOS for $(M\mathrm{As})_1/(\mathrm{GaAs})_7$, with $M =$ Cr (left column) and Mn (right column). The LSDA and LSDA + U results are shown with black-dashed and blue-solid lines, respectively.

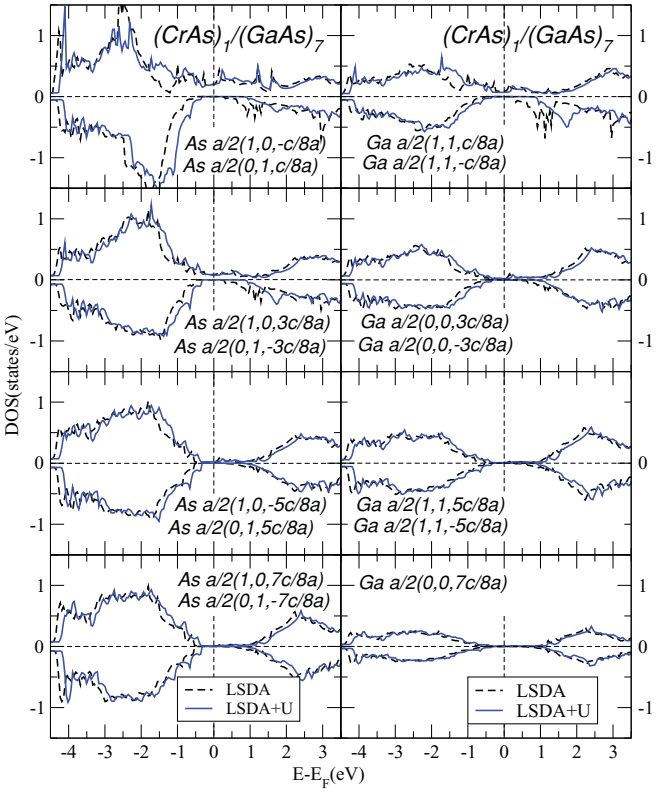

FIG. 3. (Color online) LSDA (black-dashed) and LSDA + U (blue-solid) As (left column) and Ga (right column) spin-polarized DOS for $(\mathrm{CrAs})_1/(\mathrm{GaAs})_7$. The positions in the unit cell are specified in the figures. The $U = 3$ eV and $J = 0.9$ eV parameters were used in the LSDA + U calculation.

As (Ga) DOS for the different layers. As one can see in the majority-spin channel the most important contribution around the Fermi level comes from the arsenic and gallium atoms situated at As: $a/2[1,0,c/(8a)]$, $a/2[0,1,-c/(8a)]$ and Ga: $a/2[1,1,c/(8a)]$. These are in fact the positions in the immediate vicinity of the transition metal CrAs layer. A similar trend is visible for the Mn δ-doped heterostructure in Fig. 4. In addition, we note that, as expected at the Fermi level, the dominant states are As p states. The general picture resulting from the extended analysis (by inspecting the atom and orbital resolved densities of states; see Figs. 2, 3, and 4) of the LSDA and LSDA + U results is that the δ-doped heterostructure presents a half-metallic behavior with a minority-spin gap.

LSDA + DMFT calculations were performed for the same values of $U = 3$ eV and $J = 0.9$ eV and temperatures $T = 30$, 40, and 50 K. In Fig. 5 we present the DMFT results for the atom resolved total density of states in a small energy window around E_F. Furthermore, we show the $3d$-orbital contribution into the main peaks of Cr/Mn transition metals. The insets of Fig. 5 show the results of nonmagnetic calculations, from where we can roughly estimate the bandwidth, which is about 6 eV. Based on the analysis of the values of the bandwidth, orbital occupations and the magnitude of U, one expects, for the heterostructures in discussion, a behavior typical for a medium correlated metal.

As one can see, the dynamic correlations captured by DMFT gave a completely different picture for the orbital distributions around the Fermi level. In the case of Cr, significant majority-spin density of states is obtained for the $3d_{xy}$ orbitals, in contradiction with the LSDA and LSDA + U results, where these orbitals are shown to give a negligible contribution (see Fig. 2). Above $E_F + 0.3$ eV, in the unoccupied part, the majority-spin $3d$ electrons have a significant $3d_{x^2-y^2}$ and, at higher energies (not shown), $3d_{z^2-1}$ character. In the minority-spin channel from $E_F - 0.5$ eV no significant spectral weight is present, while above E_F the many-body induced states have a predominant $3d_{xy}$ character. At higher energies a predominant $3d_{z^2-1}$ character is present.

In the case of Mn δ-doped structure, in the majority-spin channel As p is dominant at the Fermi level and the Mn-$3d_{x^2-y^2}$ contribution is seen around 0.3 eV below the Fermi level. It is interesting to note that the position of these orbitals are not changed with respect to the LSDA picture. Contrary to the LSDA, minority-spin Mn $3d_{x^2-y^2}$ have a larger spectral weight below E_F, while above E_F $3d_{xy}$ states are seen to cross the Fermi level. The general picture obtained by including

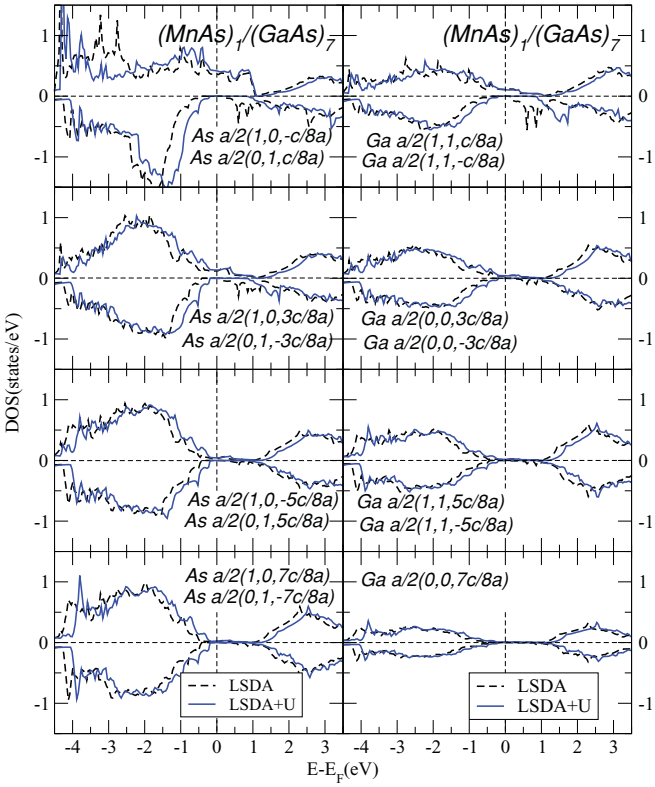

FIG. 4. (Color online) LSDA (black-dashed) and LSDA + U (blue-solid) As (Ga) spin-polarized DOS for $(MnAs)_1/(GaAs)_7$ are shown on the left (right) columns. The positions in the unit cell are specified within the figures. The $U = 3$ eV and $J = 0.9$ eV parameters were used in the LSDA + U calculation.

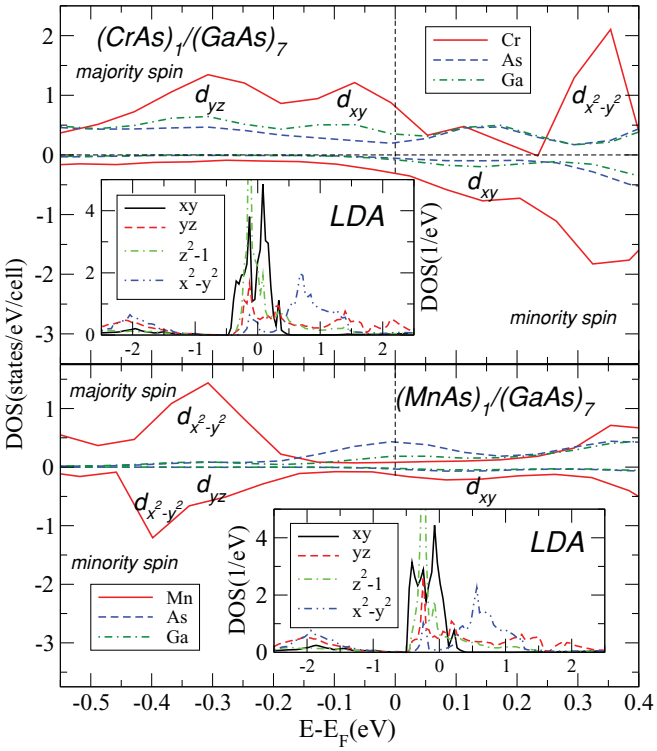

FIG. 5. (Color online) LSDA + DMFT atom resolved spin-polarized DOS for $(MAs)_1/(GaAs)_7$, with $M = $ Cr (upper panel) and Mn (lower panel). The results presented were obtained for the following parameters: $U_{Mn/Cr} = 3$ eV, $J_{Mn/Cr} = 0.9$ eV, and $T = 50$. For the correlated atoms the main orbital contributions are also shown (solid red line). Average total As (dashed blue) and average total Ga (green dot-dashed) contributions are seen also. Above E_F, many-body induced states with predominant d_{xy} character determine the closure of the half-metallic gap. Insets show the results for the orbital resolved non-spin-polarized Cr/Mn-LDA density of states.

dynamic correlations is that the gap within the minority-spin channel is closed and the half-metallicity disappears. For both Cr and Mn compounds, closure of the gap is due to the presence of many-body states with $3d_{xy}$ character only seen in DMFT.

The analysis of the orbital resolved density of states can be correlated with the behavior of the self-energy seen in Fig. 6, where the atom and orbital resolved imaginary part of self-energy is shown. The self-energies for the d_{zx} orbital were excluded since they are identical (due to the cell symmetry) to the d_{yz} self-energies. We observe that the imaginary part of the self-energy has a rather symmetric energy dependence around the Fermi level, with a normal Fermi-liquid-type behavior $\mathrm{Im}\Sigma^{\uparrow}(E)_{\mathrm{Cr/Mn}} \propto (E - E_F)^2$. The minority-spin $\mathrm{Im}\Sigma^{\downarrow}(E)_{\mathrm{Cr/Mn}}$ shows a significant increase just above the Fermi level which is more pronounced for the d_{xy} orbitals.

In Fig. 7 we plot the real part of the orbital resolved majority and minority self-energies. The left (right) columns represent the results for Cr-doped (Mn-doped) compounds. The figure also displays a line with a unitary negative slope as a guide for the analysis of the energy dependence of the real part of the self-energies around E_F. As one can see for both spin directions, the self-energy has a negative slope $\partial\Sigma(\omega)/\partial\omega$ at the Fermi energy, which confirms that the quasiparticle weight $Z = [1 - \partial\Sigma(\omega)/\partial\omega]^{-1}$ is reduced by correlations. For both Cr and Mn and for majority spins, $\partial\Sigma(\omega)/\partial\omega$ is clearly less than unity. Contrary to the minority Cr or Mn d_{xy} spins, $\partial\Sigma_{xy}(\omega)/\partial\omega$ is larger than unity above the Fermi level (within our approximation, we cannot determine it with sufficient accuracy), suggesting the nonquasiparticle nature of the minority-spin states within the gap. We have checked that the above behavior of the real and imaginary parts of the self-energy does not change significantly in the range of investigated temperatures. For smaller U values the slope is reduced slightly, although the same peculiar behavior is seen for the real and imaginary part of d_{xy} orbital self-energy. Therefore, we can conclude that the many-body induced NQP states within the minority-spin gap situated just above the Fermi level are mainly determined by the transition-metal d_{xy} orbitals. As the closure of the minority-spin gap happens by the extension of NQP-state tails from above toward the Fermi level and, in order to have a complete picture, it is important to understand the effect of correlations upon the minority-spin states situated below E_F. This can be studied by looking at the band edges within the minority-spin channel. In particular we investigate the character of the electronic states below and above E_F with or without including correlations. As discussed previously, above the the Fermi level, transition-metal $3d_{xy}$ states provide the main character that developed many-body NQP states whose tails cross E_F. Below E_F the dominant states have As p character. Therefore, we looked

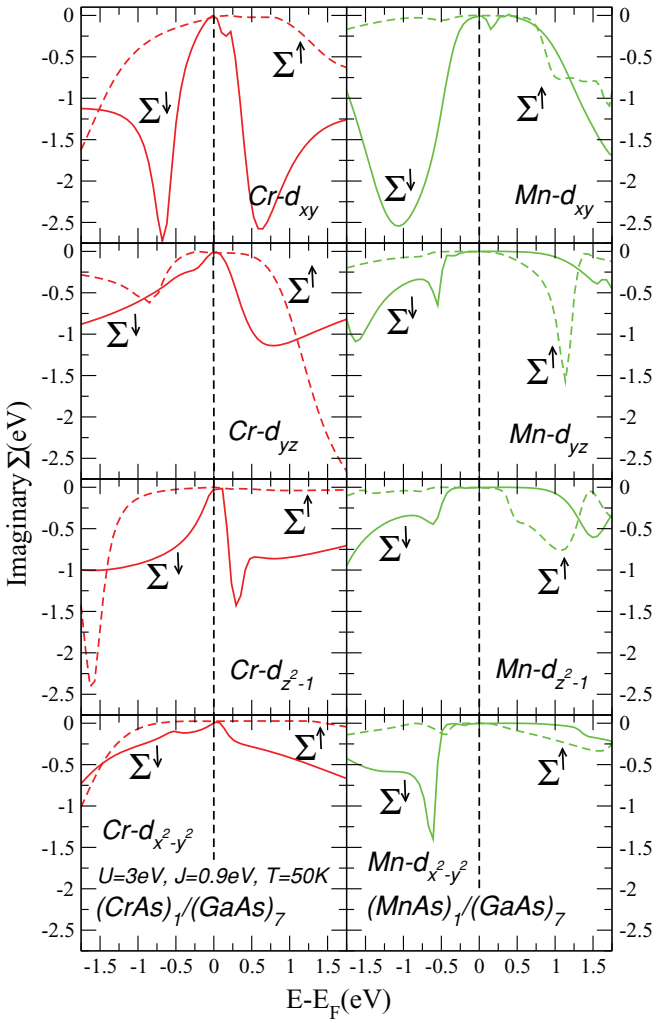

FIG. 6. (Color online) Orbital resolved imaginary part of minority-spin (majority-spin) self-energy for Cr [red solid (dashed)] and Mn [green solid (dashed)] lines computed for $U_{\mathrm{Mn/Cr}} = 3$ eV and $J = 0.9$ eV and $T = 50$ K. The hump near 0.2 eV, visible for the d_{xy} orbital, signals the departure from the expected Fermi-liquid behavior.

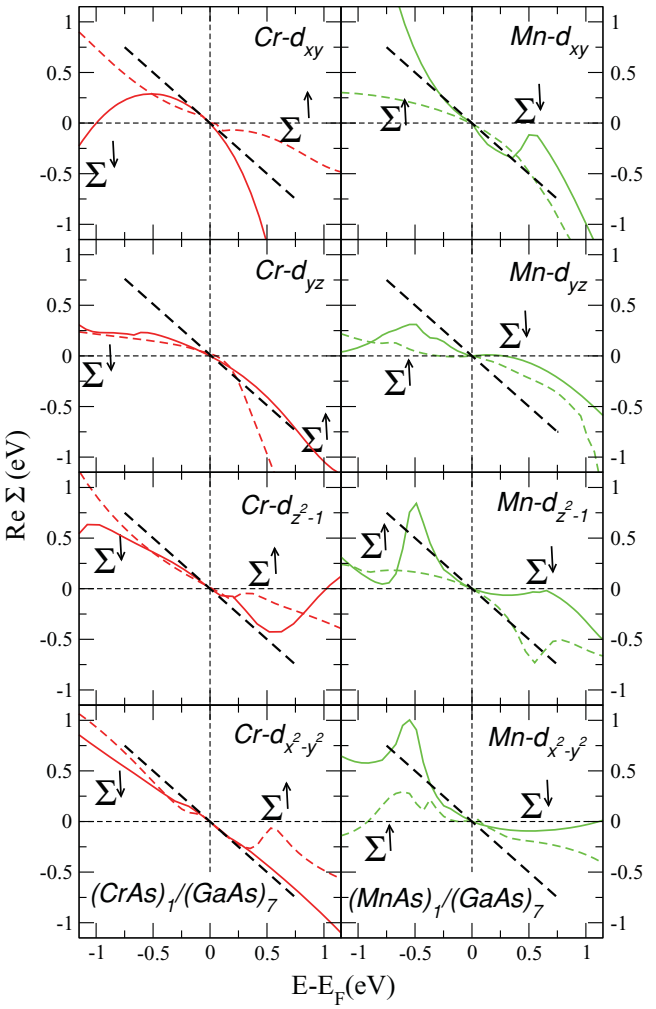

FIG. 7. (Color online) Orbital resolved real part of minority-spin (majority-spin) self-energy for Cr [red solid (dashed)] and Mn [green solid (dashed)] lines computed for $U_{\mathrm{Mn/Cr}} = 3$ eV and $J = 0.9$ eV and $T = 50$ K. A solid black line with a unitary negative slope is also shown.

at contributions of As states originating from different As layers to the top of the minority-spin valence band. The As layers are grouped into four classes, each having the distance $z_{\mathrm{As}} = \frac{a}{2}\frac{jc}{8a}$, where $j = \pm 1, \pm 3, \pm 5, \pm 7$ with respect to the transition-metal atom located at the origin. The results of this analysis is presented in Table I. As the distance between the transition metal monolayer and As monolayer increases, the As (p_x, p_y) character continues to increase. At the same time, the difference between values from different monolayers decreases. These results suggest that the As monolayer situated closer to the transition metal has its electrons confined by the p-d hybridization. At larger distances, hybridization decreases, and more p character is available to form the top of the valence band. One can note that the p_x and p_y contributions are different as a consequence of symmetry lowering, which is present in the tetragonal geometry. These results are in agreement with previous calculations obtained using the macroscopic average of the total DFT potential.[7,41,42]

In the following we comment the comparison of the results obtained within the three different approaches to the electronic structure calculations within the DFT. A well-known problem of the LSDA and its relative generalized gradient approximation (GGA) is the underestimation of the band gaps (for many semiconductors) in addition to the missing electronic correlation effects. For the heterostructures under discussion, we present results obtained with different methods that consider correlations effects: a simplified mean-field LSDA + U and a more complex LSDA + DMFT approach. The LSDA + U scheme seeks to correct the problems of the LSDA by adding a repulsive potential $+U$, obtained from a mean-field decoupling of the local Coulomb interaction. Its consequence is that the occupied (unoccupied) 3d levels are shifted to lower (higher) energies, as seen in Figs. 2, 3, and 4. The ground-state picture resulting from both of these methods is a half-metallic ferromagnetic state.

Contrary to the mean-field methods, DMFT captures correctly the dynamics at low as well as high energies. This approach properly describes the quasiparticle formation

TABLE I. Relative contribution (in percent) of the As p states to the valence band maxima from each As-layer obtained within the LSDA calculation. Local correlation within the mean-field LSDA + U or DMFT does not change significantly these values.

	$(CrAs)_1/(GaAs)_7$		$(MnAs)_1/(GaAs)_7$	
	p_x %	p_y %	p_x %	p_y %
As1: $\frac{a}{2}(0,1,\frac{c}{8a})$	10.14	16.66	10.11	17.23
As1: $\frac{a}{2}(1,0,-\frac{c}{8a})$				
As2: $\frac{a}{2}(0,1,\frac{3c}{8a})$	27.57	22.22	27.03	20.43
As2: $\frac{a}{2}(1,0,-\frac{3c}{8a})$				
As3: $\frac{a}{2}(0,1,\frac{5c}{8a})$	30.43	30.55	30.18	31.70
As3: $\frac{a}{2}(1,0,-\frac{5c}{8a})$				
As4: $\frac{a}{2}(0,1,\frac{7c}{8a})$	32.88	30.55	32.66	30.64
As4: $\frac{a}{2}(1,0,-\frac{7c}{8a})$				

around the Fermi level simultaneously with the lower and upper Hubbard bands at higher energies.[18,19] Dynamical correlations captured by DMFT change completely the physical picture of these compounds. For the majority-spin states, a slight spectral-weight redistribution takes place; however, this does not affect the value at the Fermi level which is similar to that obtained within LSDA (see Fig. 1). For minority spins, although the position of the top of the minority-spin valence band is slightly changed, including correlations, the As p contributions from different As layers are similar in value to those obtained within the LSDA calculations; see Table I. This demonstrates that the As p character distribution within the top of the minority-spin valence band is not sensitive to correlation effects. The conclusion, therefore, is that the many-body interactions affect the half-metallic band structure predominantly within the minority-spin channel above E_F by introducing NQP states. The presence of these many-body states reduces significantly the ideal 100% carrier-spin polarization predicted by LSDA(+ U). In order to discuss quantitatively the conduction-electron-spin polarization we use the common definition:[43–45] $P_n = [N_\uparrow(E_F)v_\uparrow^n(E_F) - N_\downarrow(E_F)v_\downarrow^n(E_F)]/[N_\uparrow(E_F)v_\uparrow^n(E_F) + N_\downarrow(E_F)v_\downarrow^n(E_F)]$, where N and v are the density of states and the velocity at E_F. The values of n determine what type of experimental measurements that can access the polarization. The quantity P_0 corresponds to the spin-resolved photoemission experiments, while the higher orders correspond to spin polarizations measured with point contact Andreev reflection in the ballistic ($n = 1$) or diffusive ($n = 2$) regimes.[43,44] In Fig. 8 we show the results for the polarization obtained using the simplified $P_{\mathrm{DMFT}}(E_F,T) = P_{n=0}$, where the velocities for spin up and down are dropped. One can see a clear distinction between the different temperature behavior of magnetization and polarization, similar to many potential HMF.[29,33,42,46,47]

In Table II we present the values of the finite-temperature magnetizations; the values of polarization are easily readable from the lower panel of Fig. 8. For the Mn δ-doped GaAs, the temperature dependence of remnant magnetization of samples that consist of 100 period of GaAs (10 monolayers)/MnAs (0.5 monolayers) showed a quasilinear dependence and a

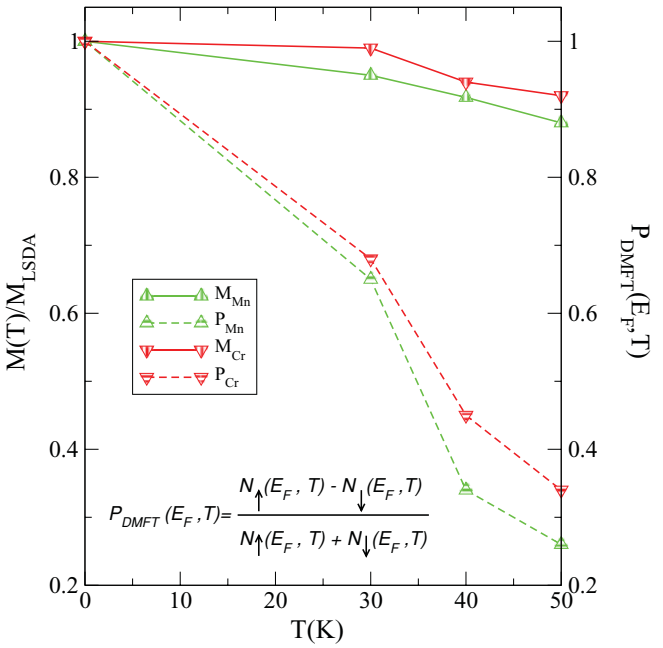

FIG. 8. (Color online) LSDA + DMFT values for the finite-temperature magnetization and spin polarization of $(M\mathrm{As})_1/(\mathrm{GaAs})_7$, M = Cr, Mn compounds. The LSDA values are taken as $T = 0$ K results.

critical temperature of about $T_c \approx 50$ K.[15] More recent measurements on the Mn δ-doped DFH include polarized neutron reflectometry and magnetometry performed on samples having 20, 50, and 100 monolayer GaAs spacers in the temperature range from 30 to 40 K.[48] This analysis allowed us to identify two types of contributions to the magnetization of Mn-doped DMH: one type that has the superlattice periodicity and the second type resulting from random clustering effects suggested by the discontinuous nature of the quasi-two-dimensional MnAs.[48] A direct comparison with these experimental results are not possible for the present theoretical calculations, due to the fact that the supercells considered here contain a considerably smaller number of layers. Nevertheless, certain qualitative agreements are obvious. As one can see in Fig. 8 the present LSDA + DMFT calculation captures a qualitative quasilinear temperature dependence of the reduced $M(T)/M_{\mathrm{LSDA}}$ magnetization also for the smaller numbers of monolayers in discussion, a behavior that is seen in the experiment. In addition, the quasi-two-dimensional nature of the problem is reflected in the present calculations by the separation of electrons and holes among different layers (see

TABLE II. Integer magnetic moment values were obtained within LSDA and LSDA + U. The finite temperature DMFT magnetic moments demonstrate departure from the half-metallic values.

	M_{LSDA}	$M_{\mathrm{LSDA}+U}$	M_{DMFT}		
	μ_B	μ_B	30 K	40 K	50 K
$(CrAs)_1/(GaAs)_7$	3.00	3.00	2.97	2.82	2.76
$(MnAs)_1/(GaAs)_7$	4.00	4.00	3.80	3.67	3.52

Table I and the discussion below). A major difference is that, for the current supercell geometry, our estimate for the Curie temperature is around four times larger.

Let us further comment upon the recent polarization measurements of spin carriers in Mn δ-doped GaAs compounds using hot-electron photoluminescence (HPL).[17] The hot-electron photoluminescent spectra were interpreted based on the previous analysis performed in diluted magnetic semiconductors.[49] According to this analysis, in Mn-doped GaAs and for a wide range of Mn content, the valence-band holes predominantly occupy the Mn-acceptor impurity band. It was suggested that the polarization of the valence-band holes is proportional to the sample magnetization.[17,49] To interpret the data on digital Mn/GaAs heterostructures, a combined contribution from the δ-doped and the unintentionally doped interlayer region was considered as a superposition of both contributions. It was shown that carriers experience a strong exchange interaction with the ferromagnetic interfaces, which rapidly decease with increasing distance with respect to the ferromagnetic Mn-δ layer.[17]

As one can see, the electronic correlations play an important role in the properties of the defect-free DMH presented above. In the presence of dynamical many-body correlations the top of the valence band does not change significantly; however, NQP states appear in the minority-spin channel (Figs. 1 and 5) just above the Fermi level. At finite temperatures the tails of the NQP states cross the Fermi level and the half-metallicity is lost. In addition, we have shown that the carriers' spin polarization and magnetization follow a different temperature behavior. We expect that optically excited radiative recombination of electrons and holes within the minority-spin channel would help to demonstrate the presence of the many-body effects; in particular the existence of nonquasiparticle states in these materials. Hot-electron photoluminescence spectroscopy was recently used to discuss hole spin polarization in diluted magnetic semiconductors.[50] The HPL circular polarization under circularly polarized excitation provides detailed information on the spin-relaxation mechanism,[49,51] and allows a finite-temperature characterization of the HPL polarization.[50] We believe that such experiments would demonstrate a different finite-temperature behavior of magnetization and polarization as qualitatively demonstrated in Fig. 8.

IV. CONCLUSIONS

The technology based on the digital-alloy technique is expected to produce heterostructures with an enhanced T_C because of locally confined high transition-metal concentration, and a better control of the ferromagnetic properties by controlling the GaAs layer thickness. The expected enhancement of the Curie temperature has not yet been realized; instead, it was found that magnetic properties depend strongly on interlayer thickness.[15,48] The results of our electronic structure calculations based on LSDA predict that the defect-free delta-doped digital magnetic heterostructures are half-metals, in agreement with previous calculations.[7] The same conclusion is given by computations that use a mean-field LSDA + U approach. Conversely, when many-body correlations captured by DMFT are included, the half-metallicity is lost. The computed finite-temperature magnetization follows an almost linear temperature dependence, similar to the experimental measurements performed for larger GaAs (10 monolayers)/MnAs (0.5 monolayers) heterostructures.[15,48] In comparing the critical temperatures, our results overestimate by a factor of four the measured values. Certainly additional work is necessary in this direction; in particular to extend the theoretical approach to include dynamical correlations beyond locality. Of particular importance in applications of DMH to spintronic devices is the effect of the ferromagnetic layers on the spin polarization of the carriers. Our results demonstrate that magnetization and polarization follows a different temperature dependence. We suggest that such an effect might be captured by hot-electron photoluminescence spectroscopy. The quantitative analysis of the intensity of recombination radiation for transitions between the electrons and holes within the minority-spin channel in the presence of electronic correlations is in progress.

ACKNOWLEDGMENTS

L.C. and E.-V.M. acknowledge the support from the PN II ID_672/2008 grant and the FWF projects no. P19630-N16, no. P18551-N16, and no. P21289 and by the cooperation project NAWI Graz Grant No. F-NW-515-GASS. L.V. acknowledges the financial support from the Swedish Research Council and the Hungarian Scientific Research Fund (research projects OTKA 84078).

[1] S. A. Crooker, D. A. Tulchinsky, J. Levy, D. D. Awschalom, R. Garcia, and N. Samarth, Phys. Rev. Lett. **75**, 505 (1995).
[2] D. D. Awschalom and N. Samarath, J. Magn. Magn. Mater. **200**, 130 (1999).
[3] K. W. Edmonds, P. Bogusławski, K. Y. Wang, R. P. Campion, S. N. Novikov, N. R. S. Farley, B. L. Gallagher, C. T. Foxon, M. Sawicki, T. Dietl, M. Buongiorno Nardelli, and J. Bernholc, Phys. Rev. Lett. **92**, 037201 (2004).
[4] W. Limmer, A. Koeder, S. Frank, V. Avrutin, W. Schoch, R. Sauer, K. Zuern, J. Eisenmenger, P. Ziemann, E. Peiner, and A. Waag, Phys. Rev. B **71**, 205213 (2005).
[5] Y. D. Park, J. D. Lim, K. S. Suh, S. B. Shim, J. S. Lee, C. R. Abernathy, S. J. Pearton, Y. S. Kim, Z. G. Khim, and R. G. Wilson, Phys. Rev. B **68**, 085210 (2003).
[6] T. Jungwirth, J. Mašek, J. Sinova, and A. H. MacDonald, Phys. Rev. B **68**, 161202 (2003).
[7] S. Sanvito, Phys. Rev. B **68**, 054425 (2003).
[8] J. L. Xu and M. van Schilfgaarde, Phys. Rev. B **74**, 241304 (2006).
[9] X. Wang, X. Chen, X. Zhou, and W. Lu, J. Phys. D **42**, 025002 (2009).
[10] M. C. Qian, C. Y. Fong, and W. E. Pickett, J. Appl. Phys. **99**, 08D517 (2006).
[11] M. C. Qian, C. Y. Fong, K. Liu, W. E. Pickett, J. E. Pask, and L. H. Yang, Phys. Rev. Lett. **96**, 027211 (2006).
[12] H. Wu, P. Kratzer, and M. Scheffler, Phys. Rev. Lett. **98**, 117202 (2007).
[13] M. Marques, L. G. Ferreira, L. K. Teles, L. M. R. Scolfaro, J. Furthmüller, and F. Bechstedt, Phys. Rev. B **73**, 224409 (2006).

[14]T. Jungwirth, J. Sinova, J. Mašek, J. Kučera, and A. H. MacDonald, Rev. Mod. Phys. **78**, 809 (2006).
[15]R. K. Kawakami, E. Johnston-Halperin, L. F. Chen, M. Hanson, N. Guébels, J. S. Speck, A. C. Gossard, and D. D. Awschalom, Appl. Phys. Lett. **77**, 2379 (2000).
[16]M. I. Katsnelson, V. Y. Irkhin, L. Chioncel, A. I. Lichtenstein, and R. A. de Groot, Rev. Mod. Phys. **80**, 315 (2008).
[17]V. F. Sapega, A. Trampert, and K. H. Ploog, Phys. Rev. B **77**, 245301 (2008).
[18]G. Kotliar and D. Vollhardt, Phys. Today **57**, 53 (2004).
[19]G. Kotliar, S. Y. Savrasov, K. Haule, V. S. Oudovenko, O. Parcollet, and C. A. Marianetti, Rev. Mod. Phys. **78**, 865 (2006).
[20]K. Held, Adv. Phys. **56**, 829 (2007).
[21]M. I. Katsnelson and A. I. Lichtenstein, Eur. Phys. J. B **30**, 9 (2002).
[22]L. Vitos, Phys. Rev. B **64**, 014107 (2001).
[23]L. Chioncel, L. Vitos, I. A. Abrikosov, J. Kollar, M. I. Katsnelson, and A. I. Lichtenstein, Phys. Rev. B **67**, 235106 (2003).
[24]M. Imada, A. Fujimori, and Y. Tokura, Rev. Mod. Phys. **70**, 1039 (1998).
[25]N. E. Bickers and D. J. Scalapino, Ann. Phys. (NY) **193**, 206 (1989).
[26]M. I. Katsnelson and A. I. Lichtenstein, J. Phys. Condens. Matter **11**, 1037 (1999).
[27]V. M. Galitskii, J. Exptl. Theoret. Phys. (USSR) **34**, 1011 (1958) [Sov. Phys.-JETP **34**, 698 (1958)].
[28]J. Kanamori, Prog. Theor. Phys. **30**, 275 (1963).
[29]L. Chioncel, M. I. Katsnelson, R. A. de Groot, and A. I. Lichtenstein, Phys. Rev. B **68**, 144425 (2003).
[30]H. Allmaier, L. Chioncel, E. Arrigoni, M. I. Katsnelson, and A. I. Lichtenstein, Phys. Rev. B **81**, 054422 (2010).
[31]L. Chioncel, P. Mavropoulos, M. Ležaić, S. Blügel, E. Arrigoni, M. I. Katsnelson, and A. I. Lichtenstein, Phys. Rev. Lett. **96**, 197203 (2006).
[32]L. Chioncel, M. I. Katsnelson, G. A. de Wijs, R. A. de Groot, and A. I. Lichtenstein, Phys. Rev. B **71**, 085111 (2005).
[33]L. Chioncel, E. Arrigoni, M. I. Katsnelson, and A. I. Lichtenstein, Phys. Rev. B **79**, 125123 (2009).
[34]D. M. Edwards and J. A. Hertz, J. Phys. F **3**, 2191 (1973).
[35]V. I. Anisimov, F. Aryasetiawan, and A. I. Lichtenstein, J. Phys. Condens. Matter **9**, 767 (1997).
[36]I. Yang, S. Y. Savrasov, and G. Kotliar, Phys. Rev. Lett. **87**, 216405 (2001).
[37]A. G. Petukhov, I. I. Mazin, L. Chioncel, and A. I. Lichtenstein, Phys. Rev. B **67**, 153106 (2003).
[38]A. I. Lichtenstein, M. I. Katsnelson, and G. Kotliar, Phys. Rev. Lett. **87**, 067205 (2001).
[39]J. S. Griffith, *The Theory of Transition-Metal Ions* (University Press, Cambridge, 1964).
[40]F. Aryasetiawan, M. Imada, A. Georges, G. Kotliar, S. Biermann, and A. I. Lichtenstein, Phys. Rev. B **70**, 195104 (2004).
[41]S. Sanvito and N. A. Hill, Phys. Rev. Lett. **87**, 267202 (2001).
[42]L. Chioncel, I. Leonov, H. Allmaier, F. Beiuşeanu, E. Arrigoni, T. Jurcuţ, and W. Pötz, Phys. Rev. B **83**, 035307 (2011).
[43]I. I. Mazin, Phys. Rev. Lett. **83**, 1427 (1999).
[44]M. S. Bahramy, P. Murugan, G. P. Das, and Y. Kawazoe, Phys. Rev. B **75**, 054404 (2007).
[45]A. Stroppa, G. Kresse, and A. Continenza, Appl. Phys. Lett. **93**, 092502 (2008).
[46]L. Chioncel, E. Arrigoni, M. I. Katsnelson, and A. I. Lichtenstein, Phys. Rev. Lett. **96**, 137203 (2006).
[47]L. Chioncel, Y. Sakuraba, E. Arrigoni, M. I. Katsnelson, M. Oogane, Y. Ando, T. Miyazaki, E. Burzo, and A. I. Lichtenstein, Phys. Rev. Lett. **100**, 086402 (2008).
[48]M. Diwekar, J. A. Borchers, K. V. O'Donovan, E. Johnston-Halperin, D. D. Awschalom, and J. Shi, J. Appl. Phys. **95**, 6509 (2004).
[49]V. F. Sapega, M. Moreno, M. Ramsteiner, L. Däweritz, and K. H. Ploog, Phys. Rev. Lett. **94**, 137401 (2005).
[50]V. F. Sapega, N. I. Sablina, I. E. Panaiotti, N. S. Averkiev, and K. H. Ploog, Phys. Rev. B **80**, 041202 (2009).
[51]V. F. Sapega, M. Ramsteiner, O. Brandt, L. Däweritz, and K. H. Ploog, Phys. Rev. B **73**, 235208 (2006).